ETH zürich

ETH Library

A toolkit for stroke infarct volume estimation in rodents

Journal Article

Author(s):
Weber, Rebecca Z.; Bernardoni, Davide; Rentsch, Nora H.; Buil, Beatriz Achón; Halliday, Stefanie; Augath, Mark-Aurel; Razansky, Daniel; Tackenberg, Christian; Rust, Ruslan

Publication date:
2024-02-15

Permanent link:
https://doi.org/10.3929/ethz-b-000657637

Rights / license:
Creative Commons Attribution 4.0 International

Originally published in:
NeuroImage 287, https://doi.org/10.1016/j.neuroimage.2024.120518

This page was generated automatically upon download from the ETH Zurich Research Collection.
For more information, please consult the Terms of use.

NeuroImage 287 (2024) 120518

Contents lists available at ScienceDirect

NeuroImage

journal homepage: www.elsevier.com/locate/ynimg

Technical Note

A toolkit for stroke infarct volume estimation in rodents

Rebecca Z. Weber [a,b], Davide Bernardoni [c], Nora H. Rentsch [a,b], Beatriz Achón Buil [a,b], Stefanie Halliday [a], Mark-Aurel Augath [d,e], Daniel Razansky [d,e], Christian Tackenberg [a,b], Ruslan Rust [a,b,f,g,*]

[a] Institute for Regenerative Medicine, University of Zurich, Schlieren 8952, Switzerland
[b] Neuroscience Center Zurich, University of Zurich and ETH Zurich, Zurich, Switzerland
[c] Department of Health Sciences and Technology, ETH Zurich, Zurich, Switzerland
[d] Institute for Biomedical Engineering and Institute of Pharmacology and Toxicology, Faculty of Medicine, University of Zurich, Zurich 8052, Switzerland
[e] Institute for Biomedical Engineering, Department of Information Technology and Electrical Engineering, ETH Zurich, Zurich 8093, Switzerland
[f] Department of Physiology and Neuroscience, University of Southern California, Los Angeles, CA 90089, United States
[g] Zilkha Neurogenetic Institute, Keck School of Medicine, University of Southern California, 1501 San Pablo St., Los Angeles, CA 900893, United States

ARTICLE INFO

Keywords:
Photothrombotic stroke
Stroke volume
Stroke size
MRI
Immunofluorescence imaging
Histology

ABSTRACT

Stroke volume is a key determinant of infarct severity and an important metric for evaluating treatments. However, accurate estimation of stroke volume can be challenging, due to the often confined 2-dimensional nature of available data. Here, we introduce a comprehensive semi-automated toolkit to reliably estimate stroke volumes based on (1) whole brains *ex-vivo* magnetic resonance imaging (MRI) and (2) brain sections that underwent immunofluorescence staining. We located and quantified infarct areas from MRI three days (acute) and 28 days (chronic) after photothrombotic stroke induction in whole mouse brains. MRI results were compared with measures obtained from immunofluorescent histologic sections of the same brains. We found that infarct volume determined by post-mortem MRI was highly correlated with a deviation of only 6.6 % (acute) and 4.9 % (chronic) to the measurements as determined in the histological brain sections indicating that both methods are capable of accurately assessing brain tissue damage (Pearson $r > 0.9$, $p < 0.001$). The Dice similarity coefficient (DC) showed a high degree of coherence (DC > 0.8) between MRI-delineated regions of interest (ROIs) and ROIs obtained from histologic sections at four to six pre-defined landmarks, with histology-based delineation demonstrating higher inter-operator similarity compared to MR images. We further investigated stroke-related scarring and post-ischemic angiogenesis in cortical peri-infarct regions and described a negative correlation between $GFAP^+$fluorescence intensity and MRI-obtained lesion size.

1. Introduction

Stroke continues to be a major cause of mortality worldwide and remains the primary cause of acquired disability, resulting in significant personal, social, and economic burdens. Although many drugs and therapies have been tested over the last decades, there is no effective strategy yet to completely prevent or cure the disease (Heart Disease and Stroke Statistics— 2016) Thrombolytic therapy using recombinant tissue-type plasminogen activator (rtPA) is the only approved drug for clinical use during the acute phase of ischemic stroke (McDermott et al., 2019) Its application, however, must be administered within 4.5 h of symptom onset to be effective, limiting the options available to patients who are unable to seek medical attention quickly. Ergo, there is an urgent need for developing new medical treatments for acute ischemic stroke. Yet, translation of preclinical stroke research is rare, which may be attributable to the lack of standardization in experimental protocols, making it difficult to compare results across studies (Lourbopoulos et al., 2021)

Rodent models have long been employed as one of the important methods for understanding ischemic stroke mechanisms. In many pre-clinical stroke studies, treatment efficacy is assessed through statistical comparison of infarct sizes of treatment versus placebo groups. Several methods are suitable to investigate the extent of brain damage in experimental stroke models. New nanotechnology-based techniques such as magnetic particle imaging (MPI) or the use of tracers (PET, SPECT) are becoming more common in preclinical research (Ludewig

* Corresponding author at: Institute for Regenerative Medicine, University of Zurich, Schlieren 8952, Switzerland.
E-mail address: rrust@usc.edu (R. Rust).

https://doi.org/10.1016/j.neuroimage.2024.120518
Received 9 October 2023; Received in revised form 9 January 2024; Accepted 11 January 2024
Available online 12 January 2024
1053-8119/© 2024 The Author(s). Published by Elsevier Inc. This is an open access article under the CC BY license (http://creativecommons.org/licenses/by/4.0/).

et al., 2017) Magnetic resonance imaging (MRI), a technique routinely applied in humans, can also be used to define ischemic lesions in rodents *in* and *ex vivo*. Nevertheless, traditional approaches using post-mortem histological examination to study the extent of neuronal death (infarct) are still considered gold standard (Mulder et al., 2017) Since this technique requires sectioning and staining of ischemic brain tissue (using 2,3,4-triphenyl tetrazolium chloride or Nissl (García-Cabezas et al., 2016; Atochin et al., 2017; Choi et al., 2018)), there is a significant concern that tissue distortion may interfere with visualization of the infarcted tissue. Histological processing can introduce changes in brain morphology (swelling/shrinkage) that affects the accuracy of lesion size measurements (Bay et al., 2021) Additionally, histological staining is manual-labor-intensive and can be subject to variability in staining intensity and interpretation leading to errors in lesion size quantification. The choice of the staining methods or the criteria used to define the lesion border can make it difficult to compare ischemic area across different studies. Moreover, there is a whole range of different calculations/estimates that are used to determine infarct area and volume. It can be done using software (e.g. FIJI software (Schindelin et al., 2012)) which might allow automatic infarct volume determination (Sommer, 2010) Otherwise, one can also manually identify regions of interest and lesion volumes can then be calculated as the sum of the sectional infarct areas multiplied by the interval thickness (Sommer, 2010)

With the development of specialized small animal scanners, magnetic resonance imaging (MRI) has more recently become a promising modality in preclinical laboratories that provides high-resolution images allowing for accurate and precise measurements of stroke size (Raylman et al., 2018) Additionally, since MRI is commonly employed in clinical practice, it is a valuable tool for translating preclinical research findings. But since MRI equipment and maintenance can be expensive, its accessibility in preclinical research is still limited. There are several protocols in development to estimate lesion volumes based on *ex vivo* MRI data, however, most require advanced expertise and commercial softwares (Gabrielson et al., 2018)

The goal of the present study was to develop a straightforward semi-automated toolkit to estimate lesion volumes of ischemic mouse brains that can be applied to both whole brain scans and brain sections. MRI was performed on formalin-fixed whole mouse brains from a photothrombotic model of stroke followed by macroscopic histological evaluation. We further set out to compare, within the same animals, infarct areas and volumes quantified from post-mortem MRI with that obtained from histological sections stained with NeuroTrace. This study shows that using our toolkit, MRI and histological evaluation both yield to comparable stroke volumes and can be used interchangeably depending on the individual experimental setup.

2. Methods & materials

2.1. Study design

Methods for measuring lesion volume were compared utilizing histology and MRI from the brains of mice ($n = 10$) that had undergone cortical ischemia. All animals received a large photothrombotic stroke to the right sensorimotor cortex. At 3 and 28 days after injury induction, whole heads were collected, formalin-fixed and imaged using T2-weighted MRI. Brains were removed, dissected, and histologically analyzed. We chose the timepoints based on previous literature (Bogaert-Buchmann et al., 2013); animals were categorized according to the phase of stroke as acute (<3 days post-stroke, $n = 6$) or chronic (≥28 days post-stroke, $n = 4$).

2.1.1. Animals

All procedures were conducted in accordance with governmental, institutional (University of Zurich), and ARRIVE guidelines and had been approved by the Veterinarian Office of the Canton of Zurich (ethics approval code: 209/2019). In total, 10 adult female C57BL/6 mice (acute timepoint: $n = 6$, chronic timepoint: $n = 4$) were used. Breeding of C57BL/6 mice was performed at Laboratory Animal Services Center (LASC) in Schlieren, CH. All animals were housed in standard type II/III cages on a 12 h day/light cycle (6:00 A.M. lights on) with food and water ad libitum. All mice were acclimatized for at least a week to environmental conditions before set into experiment.

2.1.2. Photothrombotic stroke induction

Anesthesia was performed using isoflurane (5 % induction, 1.5–2 % maintenance, Attane, Provet AG) and adequate sedation was confirmed by tail pinch. Novalgin (1 mg/ml) was applied via drinking water; 24 h prior to the procedure and for three consecutive days directly after stroke surgery. Cerebral ischemia was induced by photothrombotic stroke surgery as previously described (Weber et al., 2020; Rust et al., 2019; Rust et al., 2019; Fan et al., 2023; Weber et al., 2022; Rust et al., 2022) Briefly, animals were fixed in a stereotactic frame (David Kopf Instruments), the surgical area was sanitized using betadine (Mundipharma, Germany), and the skull was exposed through a cut along the midline. A cold light source (Olympus KL 1,500LCS, 150 W, 3020 K) was positioned over the right forebrain cortex (anterior/posterior: −1.5–+1.5 mm and medial/lateral 0 mm to +2 mm relative to Bregma). Rose Bengal (15 mg/ml, in 0.9 % NaCl, Sigma) was injected intraperitoneally 5 min prior to illumination and the region of interest was subsequently illuminated through the intact skull for 10 min. To restrict the illuminated area, an opaque template with an opening of 3 × 4 mm was placed directly on the skull. The wound was closed using a 6/0 silk suture and animals were allowed to recover.

2.1.3. Blood perfusion by Laser Doppler imaging

Cortical perfusion was evaluated using Laser Doppler Imaging (Moor Instruments, MOORLDI2-IR). Briefly, animals were fixed in a stereotactic frame and the region of interest was shaved and sanitized. A cut was made along the midline to uncover the skull, and the brain was scanned using the *repeat image measurement* mode. The resulting data was exported and quantified using Fiji (Image J) in terms of total flux in the ROI.

2.1.4. Sample preparation

Animals were euthanized using pentobarbital (i.p, 150 mg/kg body weight, Streuli Pharma AG) and transcardially perfused with Ringer solution (containing 5 ml/l Heparin, B. Braun) followed by paraformaldehyde (PFA, 4 %, in 0.2 M phosphate buffer, pH 7). For MRI procedure, whole mouse heads were collected and post-fixed in 4 % paraformaldehyde (PFA) solution for 36 h.

2.1.5. MRI protocol

T2-weighted images were acquired on a 7T small animal scanner with 16 cm bore size (Bruker, Ettlingen, Germany). The fixed brains were put into an Eppendorf cap filled with perfluoropolyether (Fomblin Y, Sigma-Aldrich, Switzerland) and imaged using a cryogenically cooled quadrature surface coil (Bruker, Fällanden, Switzerland). A package of 20 slices with 0.3 mm thickness (no interslice gap) was acquired with a FLASH sequence with a field of view of 15 mm x 15 mm and matrix size of 300×240, yielding a spatial in-plane resolution of 50 μm x 50 μm (echo time TE=10 ms, repetition time TR=400 ms, 10 repetitions, total scan time 10 min 40 s).

2.1.6. Histology

After MRI acquisition, brains were removed and transferred to 30 % sucrose for 3 consecutive days for cryoprotection. Coronal sections were cut (40um, Microm HM430, Leica) and kept as free-floating sections in a cryoprotectant solution (PBS, ethylene glycol, sucrose) at −20 °C. For immunostainings, sections were blocked with 5 % normal donkey serum for 1 h at room temperature and incubated with NeuroTrace (1:2000, in 0.1 M PB, Sigma) for 30 min. Sections were mounted using Mowiol.

2.1.7. Data processing

The estimation of lesion volumes was divided into 3 stages. In the first stage, the lesion area was manually traced/outlined on each coronal brain section (MRI images and NeuroTrace-stained images) using FIJI (*ImageJ*, version 2.1.0/1.53c). In the second stage, once regions of the lesion have been identified, numerical values for the number of pixels in the selection were obtained and converted into mm (McDermott et al., 2019). In the third stage, these values were imported into MATLAB (R2022a, The Mathworks, Natick, MA, USA) and lesion volumes were calculated using a customized script. For step-by-step guidance, please refer to our protocol (Supplementary Materials).

2.1.8. Image pre-processing

Neurotrace-stained sections were visualized using an Axio Scan Z.1 slide scanner (Carl Zeiss, Germany) with a 20x/0.8 objective lens and later processed and exported as -.tiff files using the ZenBlue software (Version 3.5, Carl Zeiss, Germany). Each histologically processed slice could be matched with the corresponding *ex vivo* MRI slice using the mouse brain atlas and easily identifiable brain structures, such as white matter tracts (e.g. anterior commissure, corpus callosum, medial lemniscus), the periaqueductal gray and ventricles as anatomical landmarks (Sergejeva et al., 2015) Once matched, each fluorescence brain slice was registered to the corresponding *ex vivo* MRI slice using a 2D affine transformation. We used a tool provided by Fiji (Landmark Correspondences) (Saalfeld and Tomancak) Landmarks for registration were selected manually by a qualified researcher. We used points that were easily recognizable on both modalities, such as structure intersections, corners, and intact slice edges. We used 20 landmarks per average for the registration for each brain slice.

2.2. Lesion area measurement

The infarcted areas were estimated by a blinded researcher using the software FIJI (ImageJ, version 2.1.0/1.53c). On each brain section (MRI and NeuroTrace-stained), the ischemic area was visually identified as defined by elevated T2 values (with respect to healthy brain tissue) for MR images and areas with atypical and atrophic tissue morphology including pale areas with lost NeuroTrace staining for histological images. For MRI analysis, the threshold was determined as the mean of average T2 values within a ROI in the unaffected, contralateral cortex for both groups of animals (3dpi and 28dpi). High intensity values above the threshold were selected. The identified ischemic area was then manually delineated using the freehand polygon tool. On the NeuroTrace images, the ischemic lesions with hyperintense signal, compared to mean fluorescence intensity in a ROI in the unaffected, contralateral cortex, were visually determined and outlined. All outlined ROIs were measured (numerical value for the number of pixels) and converted to mm (McDermott et al., 2019) using an index ruler of known size which was included beforehand. Values were stored in a *.-csv* table.

Image processing for method validation was performed by two blinded and qualified researchers. Each researcher manually delineated ROIs at defined landmarks on a subset of 4 brains in total (acute: $n = 2$, chronic: $n = 2$). NeuroTrace-stained brain sections were analyzed for the depth of the cortical lesion at three defined landmarks (−0.3, 0 and 1 mm in relation to bregma).

2.3. Volume estimation

Once the lesion area in each slice was estimated, the lesion volume was calculated using a customized MATLAB script (see Suppl. Materials). We used the *modified akima interpolation* (makima) function to interpolate the missing values. The area under the curve (AUC) was calculated using the trapezoidal computation rule. Briefly, the volume was calculated by multiplication of the lesion area and the distance between the sections as follows:

$$\int_a^b f(x)dx \approx (b-a)\frac{f(a)+f(b)}{2}$$

$f(x)$ represents the cross-sectional area at x.

2.4. Histological quantification of vasculature and astrogliosis

All analysis steps were performed in a peri-infarct region distal to the stroke core with a width of 300 μm. Post-ischemic angiogenesis was assessed using the software FIJI (ImageJ, version 2.1.0/1.53c) and a script that allows to automatically calculate (1) vascular density, (2) number of branches and junctions and (3) the length of blood vessels (Rust et al., 2019) The glial scar signal intensity was calculated from 3 brain sections per animal immunostained for GFAP. Images were converted into 8-bit format and thresholded based on mean grey values obtained from ROIs in the unaffected contralateral cortex to get a binarized image. The total area of the reactive gliosis surrounding the ischemic lesion was then calculated.

2.5. Statistics

Statistical analysis was performed using R-Studio. Sample sizes were designed with adequate power according to previous studies. All data were tested for normal distribution by using the Shapiro-Wilk test. The significance of mean differences between normally distributed data (MRI vs. Histology) were tested for differences with a two-tailed paired two-sample *t*-test. The significance of mean differences between two different timepoints (acute vs. chronic) was tested for differences using an unpaired two-sample *t*-test or a one-way ANOVA with post-hoc analysis (p **adjustment** method = holm), in case of multiple comparisons. Variables exhibiting a skewed distribution were transformed, using natural logarithms before the tests to satisfy the prerequisite assumptions of normality. To assess the relationships between MRI-based and histology-based assessments, correlation analysis was performed using the Pearson correlation coefficient (r). Data are expressed as means ± SD, and statistical significance was defined as $^{*}p < 0.05$, $^{**}p < 0.01$, and $^{***}p < 0.001$.

3. Results

We developed a comprehensive step-by-step guide that offers a reliable method for accurately determining stroke volume based on data acquired by post-mortem MRI and histology (Fig. 1).

We induced a photothrombotic stroke in the right sensorimotor cortex in C57BL/6 mice (Fig. 2A). Successful stroke induction was verified using Laser Doppler imaging (LDI, Fig. 2B) confirming severe cortical blood flow reduction of more than 70 % compared to baseline levels in the lesioned hemisphere directly after surgery (acute = −71.8 %, chronic = −71.7 %, $p = 0.98$, Fig. 2C, Suppl. Table 1). Brain tissue was collected at two different time points: acutely at 3 days post injury (dpi) and at chronic stages, 28 dpi. After perfusion, whole heads were preserved in 4 %-paraformaldehyde (PFA) for 36 h in preparation for the *ex vivo* MRI. After MRI acquisition, brains were removed and sliced into coronal sections to undergo histological processing.

Stroked areas and volumes were calculated based on MRI-acquired images and histologically processed sections. We used NeuroTrace, a fluorescent Nissl stain widely used to investigate morphological changes in neural tissue after experimental stroke (Gouveia et al., 2017; Wahl et al., 2017) First, coronal MRI and histological sections were matched to the same spatial location along their anteroposterior axis according to the mouse brain atlas (Reference Atlas 2023) We used easily identifiable brain structures, such as white matter tracts (e.g., anterior commissure, corpus callosum), the periaqueductal gray and ventricles as anatomical landmarks (Fig. 2D). An average of 10–20 slices per brain were sufficient

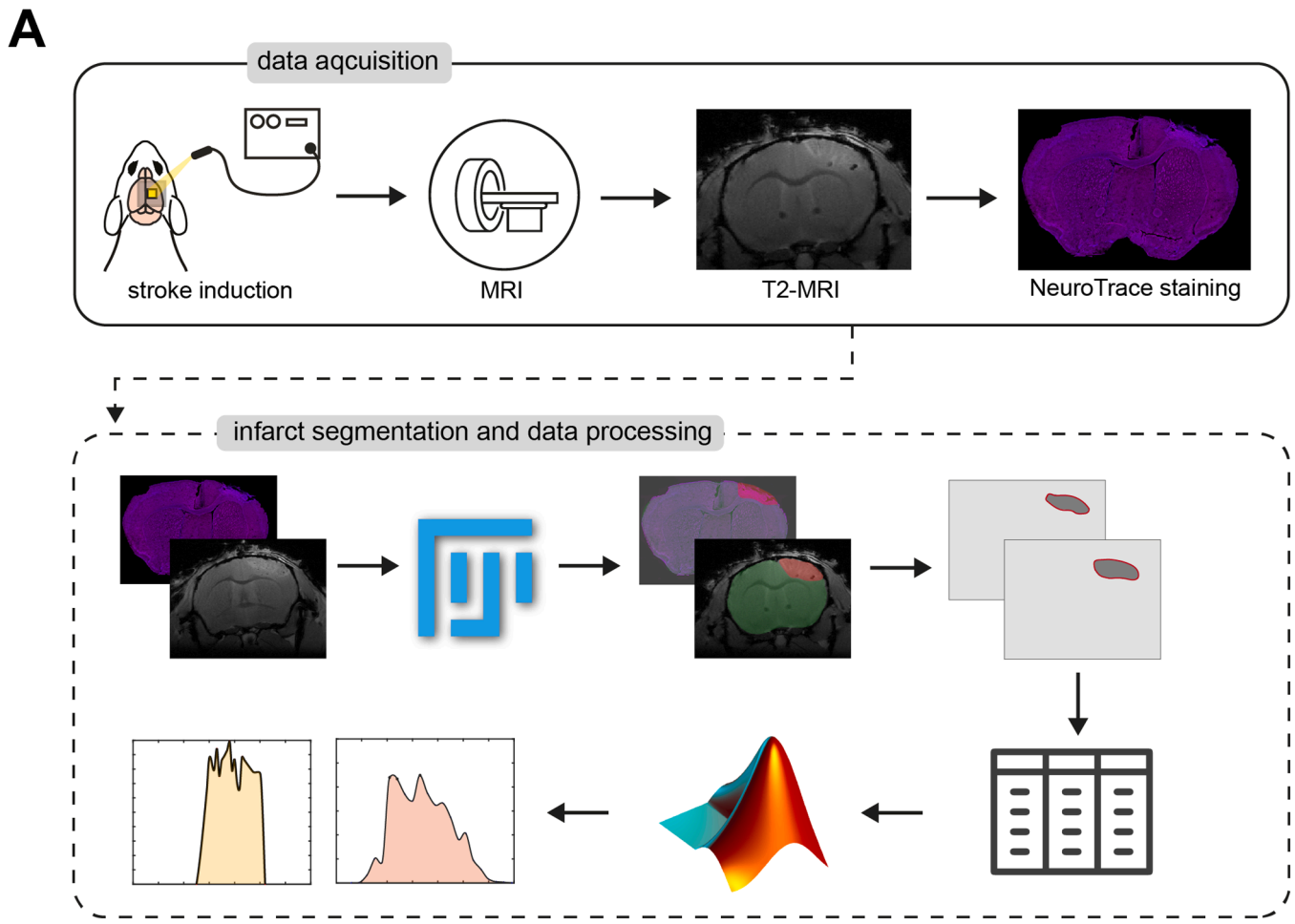

Fig. 1. Pipeline for infarct volume estimation based on *ex vivo* MRI and histology. Data acquisition (upper panel): The photothrombotic model was used for infarct induction followed by post-mortem MRI of whole heads. After MRI, brains were removed, sectioned, and histologically processed using fluorescence NeuroTrace stain. Data processing (lower panel): Lesioned areas were identified on all MRI scans and NeuroTrace-images using Fiji (ImageJ). Infarct regions of interest (ROIs) were extracted and referenced to the mouse brain atlas. Areas of all cross sections were measured using MATLAB software followed by volume quantification.

to cover the infarcted area. This value corresponds to standard MRI scans used to assess lesion volume (Koch et al., 2019) The infarcted regions were identified by abnormal signal intensity and the clear contrast between the normal and the infarcted, atrophic zone (Fig. 2E). The hyperintense morphological changes seen in the T2-MRI are indicative of brain swelling and increased water content in the stroked tissue. Brain section stained with fluorescent NeuroTrace reveal shrunken and distorted neurons. Lesioned areas were manually outlined on each section using Fiji (ImageJ) and masks of same dimensionality were exported to be further processed in MATLAB (Fig. 2F).

Areas of all cross-sections (MRI and NeuroTrace-stained images) were measured and analyzed using MATLAB. To interpolate data within the range of our measurements we used the makima (Modified Akima Method with Improved Accuracy) function (Modified Akima piecewise cubic Hermite interpolation - MATLAB makima 2023) No significant differences were observed between MRI analysis and histological analysis in quantifying lesion area for both the acute and chronic timepoints (Fig. 3A, B). However, histology-based lesion areas were consistently higher than those derived from MR images for Bregma regions +0.5 mm - +2 mm, although the differences were not significant. MRI analysis provides a higher sensitivity in identifying subtle changes in tissue integrity in the most rostral and caudal areas of the stroke, which may not be detected with histology. To visualize differences/correspondence of the two methods along the anterior-posterior axis, we calculated the difference for pre-defined bregma values (whereas 0 equals no difference at all, and 1 equals maximum difference observed, Fig. 3C). Dissimilarities between MRI and histological measurements where most prominent for Bregma regions −1.5 mm to −0.5 mm and around +2.5 mm for the acute timepoint and −0.5 mm to +1.5 mm for the chronic timepoint. Lesion area for acute and chronic phases obtained from MRI-based analysis correlate positively and equally well to those obtained through histological analysis (acute: Pearson $r = 0.923$, $p<0.001$; chronic: Pearson $r = 0.931$, $p<0.001$, Fig. 3D).

Next, total stroke volumes were calculated from the area under the curve (AUC) using a trapezoidal computation (Fig. 3E). No significant difference could be found between MRI-based analysis and histology for both, acute (MRI: 9.24 ± 3.09 mm (Lourbopoulos et al., 2021); histology: 9.14 ± 4.61 mm (Lourbopoulos et al., 2021), $p = 0.97$) and chronic (MRI: 1.56 ± 0.29 mm (Lourbopoulos et al., 2021); histology: 1.64 ± 0.33 mm (Lourbopoulos et al., 2021), $p = 0.73$, Suppl. Table 1) timepoints. A highly significant correlation was observed for lesion volumes obtained through MRI and histological analysis (Pearson $r = 0.908$, $p<0.001$, Fig. 3F).

Previous reports have shown that stroke size decreases between the initial (acute) and long-term (chronic) stages largely as a result of tissue distortion, phagocytosis, resolution of edema, glial and neural remodeling (Gaudinski et al., 2008). In line with expectations, we observe a comparable decrease in infarct volume between the acute (3dpi) and chronic (28dpi) timepoint (MRI = −83.2 % and histology: - 81.2 %) (Li et al., 2014; Shen et al., 2019)

The induced lesion reached into deep cortical layers (from layer IV to layer VI) across all animals. We did not observe differences between the

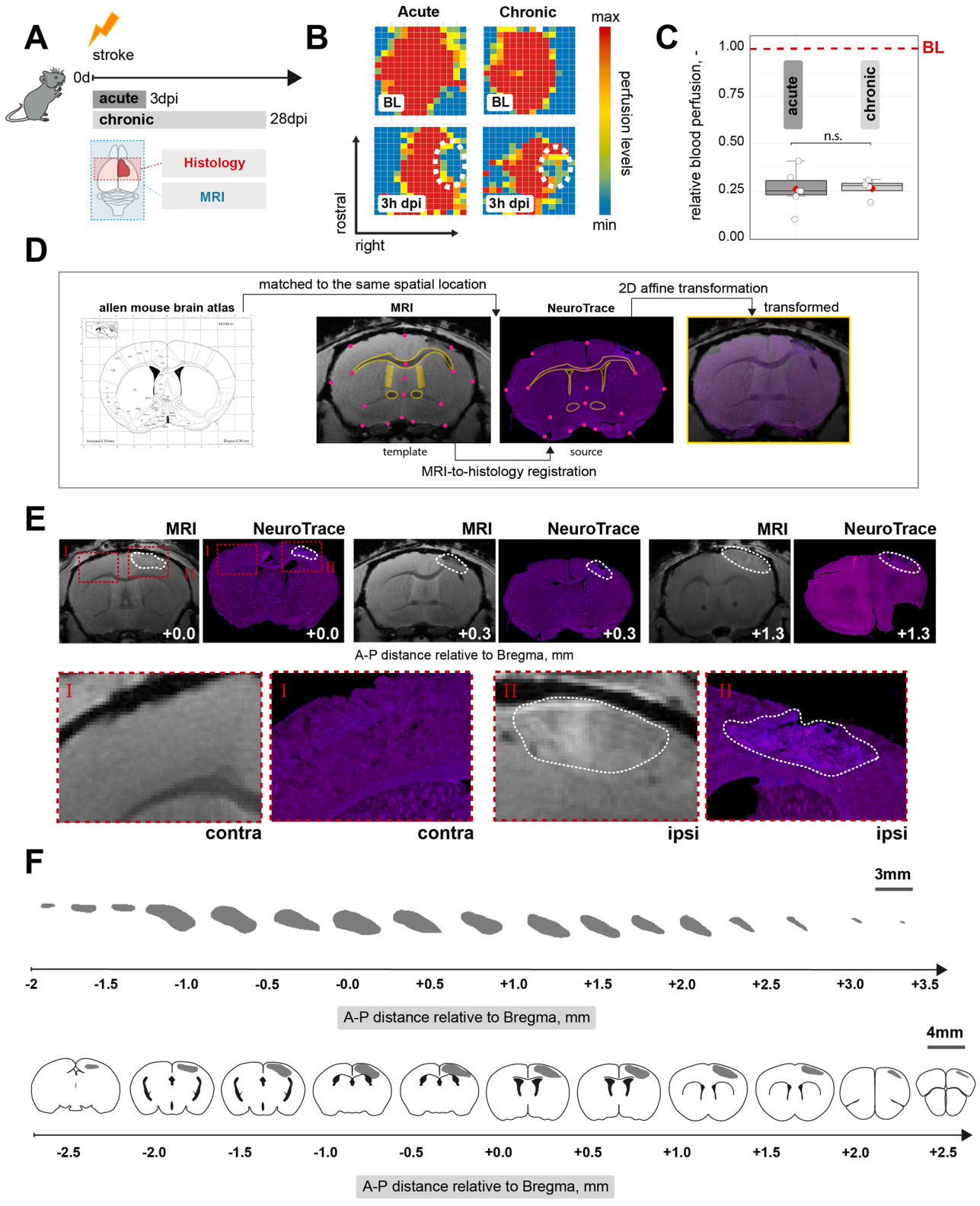

Fig. 2. Stroke induction, validation and referencing to brain atlas (A) Schematic representation of experimental set-up and groups of mice (B) Representative images of relative blood perfusion at baseline and 3 h after stroke induction (C) Quantification of cerebral blood perfusion of the injured hemisphere at 3 h following injury relative to baseline blood perfusion (D) Schematic diagram of the MRI-to-histology transformation using the Landmark Correspondence tool (E) Representative images show ischemic lesion (white outline) on MRI and NeuroTrace-stained coronal brain sections at 3 days after injury (F) Example of manually outlined and extracted infarct ROIs. The ROIs were referenced to the mouse brain atlas according to their anterior-posterior (A-P) distance to Bregma. Scale bar: 3 mm (top) and 4 mm (bottom). Boxplots indicate the 25 % to 75 % quartiles of the data. For boxplots: each dot in the plots represents one animal. Significance of mean differences between the groups (acute and chronic) was assessed using unpaired two-sample *t*-test. BL, baseline; dpi, days post injury; MRI, magnetic resonance imaging; contra, contralesional; ipsi, ipsilesional, ROI: region of interest.

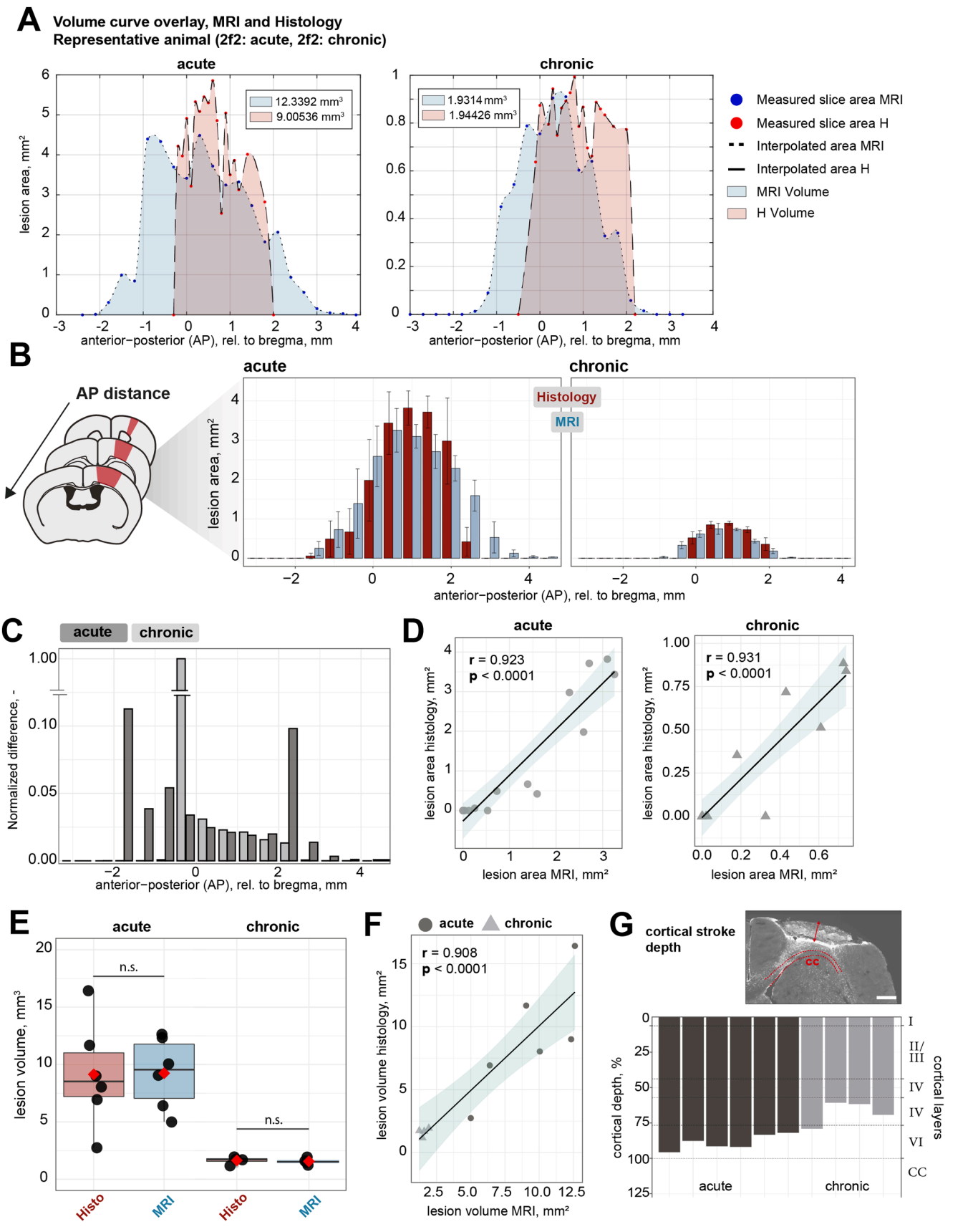

(caption on next page)

Fig. 3. Quantification of infarct volumes from MRI of whole brain tissue and histological analysis of sliced brain sections (A) Example of two volume curve overlays of both approaches (MRI and histology) at 3 and 28 days after stroke induction (B) Quantification of lesion area at day 3 and 28 after stroke induction based on MRI and histology (C) Quantification of difference between acute and chronic timepoint for defined Bregma values. Data normalized on a 0–1 range (D) Correlation analysis of stroke lesion area obtained via MRI to those obtained from NeuroTrace stained brain sections (E) Quantification of lesion volume at day 3 and 28 after stroke induction based on MRI and histology (F) Correlation analysis of stroke lesion volume obtained via MRI to those obtained from NeuroTrace stained brain sections (G) Quantification of cortical stroke depth for all individual animals at acute and chronic timepoints. Location of cortical layers I - VI is indicated with dotted lines. Scale bar: 500um. Data are shown as mean distributions where the red dot represents the mean. Boxplots indicate the 25 % to 75 % quartiles of the data. For boxplots: each dot in the plots represents one animal. Significance of mean differences between the groups (histology and MRI) was assessed using paired two-sample *t*-test, correlation analysis was performed using the Pearson correlation coefficient (r). MRI, magnetic resonance imaging; H, histology. .

individual animals within one group, but a significant decrease in lesion depth from acute (3dpi) to chronic (28dpi) timepoint (−24 %, $p < 0.001$, Fig. 3G).

To identify stroke related scarring, we quantified GFAP+ fluorescence intensities in a 300-um cortical peri-infarct region adjacent to the infarct area as well as in the contralesional cortex (Fig. 4A). Scarring signals were elevated in the ipsilesional cortex compared to contralesional regions (Fig. 4B). In peri-infarct areas, $GFAP^+$ signals were significantly elevated in the chronic group compared to the acute timepoint (+126 %, $p<0.001$). Statistical analysis between $GFAP^+$ fluorescence intensities and MRI-obtained lesion size using the Pearson correlation test revealed a no significant correlation at both timepoints (Pearson r *acute* $= -0.106$, $p>0.05$, Pearson r *chronic* $= 0.606$, $p>0.05$ Fig. 4C).

We next asked if vascular remodeling, e.g., increased vascular density after stroke may positively coincide with infarct volume decrease. We quantified vascular density, number of branches and total length of the vascular network in the peri-infarct areas (Fig. 4D, E). All parameters were normalized to their respective contralateral hemisphere. No vascular differences were observed between the acute and the chronic timepoint. Correlation analysis revealed no stable relation between CD31+ vessels and MRI-based infarct size measurements for all three parameters (vascular density, Pearson $r = -0.103$; number of branches, Pearson $r = 0.28$, length of branches, Pearson $r = 0.203$, Fig. 4F).

To quantitatively assess the similarity between the MRI-delineated ROIs and the NeuroTrace ROIs, the Dice similarity coefficient (DC) was calculated for a subset of brain sections (acute: $n = 4$, chronic: $n = 2$) at pre-defined Bregma positions (−1, −0.3, +0.8, +2 mm relative to Bregma, Fig. 5A, B). We achieved good correspondence for both timepoints (DC > 0.8). Lesion ROIs on MR and NeuroTrace images were independently reanalyzed by two blinded observers on a subset of brain sections ($n_{NeuroTrace} = 28$ and $n_{MRI} = 27$) from randomly selected animals at pre-defined Bregma positions (from −1 to +2 mm relative to Bregma). The similarity between ROI delineation by the two operators was significantly higher for NeuroTrace-stained brain sections in comparison with MR images ($DC_{NeuroTrace}$: 0.89, DC_{MRI}: 0.82, $p<0.05$), no differences were found between acute and chronic timepoints (Fig. 5C, D).

4. Discussion

In preclinical research, accurate quantification of the lesion size is crucial; it helps to assess the effectiveness of treatments and to compare results across different studies. Several methods are being used to assess stroke size, with histopathology being considered the gold standard. However, there are certain limitations that come along with this approach: Histology only provides two dimensional images, which can lead to underestimation of the true lesion extent. Secondly, brain tissue processing can cause artifacts, such as shrinkage or distortion, which can further affect the accuracy of the measurements. Additionally, histological methods can be time-consuming and labor-intensive (e.g., sectioning, staining, mounting), making it challenging to process a large number of samples. In the last decades, a vast number of new imaging tools have emerged that allow for a reliable assessment of stroke volumes. One such method is magnetic resonance imaging (MRI). MRI provides high-resolution images allowing for accurate and precise measurements of stroke size. And with the introduction of small animal scanners, it has now become a promising tool commonly used in preclinical research.

In this study, we developed a comprehensive step-by-step guide to quantify stroke volume. We employed two distinct techniques for estimating lesion area and volume in an experimental photothrombotic stroke model: (1) based on data acquired by post-mortem MRI and (2) based on a histological approach, where brain sections stained with fluorescent NeuroTrace stain reveal shrunken and distorted neurons indicating tissue necrosis. The use of perfused-fixed brains throughout the whole study allowed us to directly compare the results. Both techniques, MRI and histology, were capable of visualizing all parameters of infarction/well-defined ischemic area. And despite the mentioned confounders, such as tissue shrinkage or loss of material from the lesion core during histological processing, we found that the final infarct volume on MRI was very well correlated with the infarct volume measured on NeuroTrace-stained sections. The methodology presented in this paper is not limited solely to the photothrombotic stroke model but can be readily expanded to other experimental infarct models where visual identification of the lesioned area is possible, such as the widely used middle cerebral artery occlusion (MCAo) model or the endothelin-1 (ET-1) injection model (Pianta et al., 2019); (Vahid-Ansari et al., 2016)

In this study, we used a simple 2D-affine transform to fit the histopathology to the *ex vivo* MRI shape. For this registration, we used landmarks placed at the boundary and on pre-defined and easily identifiable internal structures of the MRI template and the histopathology source image, to find the optimal transform. Spatial localization, registration and lesion delineation was performed manually, although segmentation algorithms are available for both, histological infarct delineation and MRI (Mulder et al., 2017; McBride et al., 2016) Threshold-based semi-automated and fully automated approaches are still biased by many false-positive or -negative data, respectively. Complex algorithms underlying tissue segmentation may not accurately capture variations in image intensity and quality, potentially leading systematic errors such as over- or underestimation of lesion boundaries (Koch et al., 2019) Noise and artifacts, e.g. originating from the histological preparation, still require manual intervention to correct errors, potentially negating the time-saving advantage. On the contrary, manual segmentation allows for a more nuanced interpretation, as additional contextual information can be incorporated. A deep learning-based approach to conduct automatic stroke lesion segmentation on animal data has recently been introduced (An et al., 2023) This fully automated algorithm produces lesion segmentation that very closely resembles human annotation but also requires preprocessing steps if you deal with high signal intensity variations. These preprocessing steps are often prone to error in presence of infarcted tissue (Koch et al., 2019) Generally, deep learning based models are powered with graphics processing units (GPUs) and other infrastructure components, which can be incredibly costly. They are typically reliant on high-quality data and intensive training, and skilled personnel is needed to operate such algorithms.

To test the similarity between the MRI- and the histology-based approach, we used the dice coefficient (DC), also known by other names (Dice index or Sorensen index) (Sørensen et al., 1948) The DC is commonly utilized in brain segmentation studies to assess lesion area classification in relation to a ground truth segmentation mask (Zou et al., 2004) Here, we chose the DC to address spatial overlap between

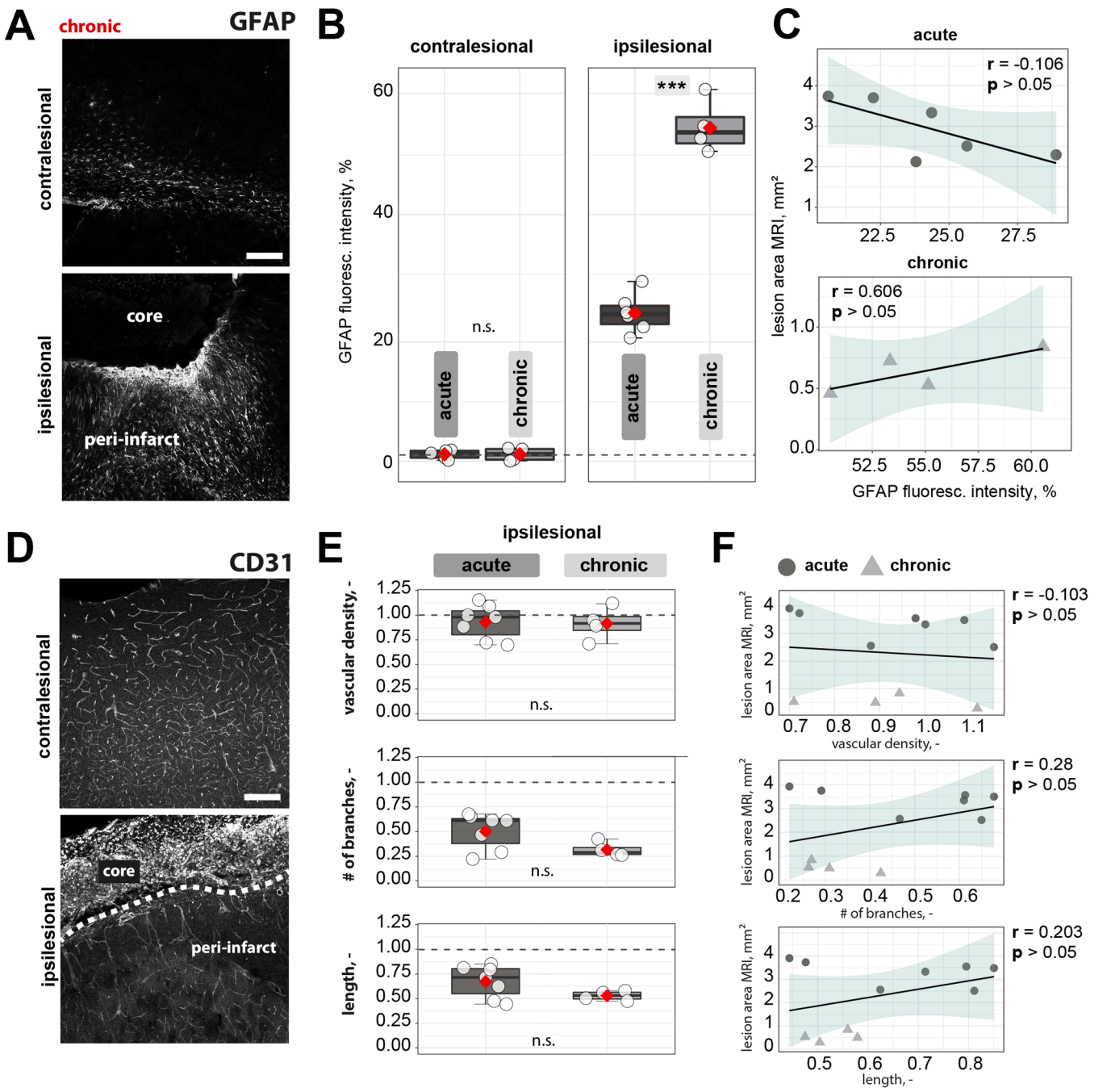

Fig. 4. Anatomical changes after stroke induction and correlation to lesion size (A) Representative histological overview of activated reactive astrocytes (GFAP$^+$). Scalebar: 100um (B) Quantification of relative GFAP$^+$for both timepoints, acute and chronic (C) Correlation analysis of stroke lesion volume obtained via MRI to relative GFAP+ expression for both timepoints, acute and chronic (D) Representative images of CD31+ vasculature in the ipsi- and contralesional cortex. Scale bar: 100um (E) Quantification of vascular density, number of vascular branches and vascular length of ipsilesional cortex for both timepoints, acute and chronic (F) Correlation analysis of stroke lesion volume obtained via MRI to vascular parameters. Data are shown as mean distributions where the red dot represents the mean. Boxplots indicate the 25 % to 75 % quartiles of the data. For boxplots: each dot in the plots represents one animal. Significance of mean differences between the groups (acute vs. chronic) was assessed using unpaired two-sample *t*-test, correlation analysis was performed using the Pearson correlation coefficient (r). MRI, magnetic resonance imaging. .

delineated lesion ROIs obtained from NeuroTrace-stained sections and MR images. Method accuracy was demonstrated in a dataset consisting of brain sections at four defined landmarks (6 brains, 24 sections in total). Validation of our method showed good accuracy for acute and chronic timepoints (DC > 0.8, whereas 0 indicates no overlap and 1 indicates perfect overlap). The correspondence between the delineated ROIs was slightly higher at chronic timepoints when the infarct boundaries were clearly identifiable by the glial scar. At acute timepoints, infarcted regions were characterized by partial tissue loss and thus, ROI boundaries were less clear. This underscores the significance of clearly defining norms for lesion delineation in advance to ensure successful application across different experimental groups.

In addition, the feasibility of the method was demonstrated in terms of the consistency between two blinded observers. We achieved good correspondence between the two observers (DI > 0.8), although the differences in ROI delineation were higher on MR images (DI = 0.82)

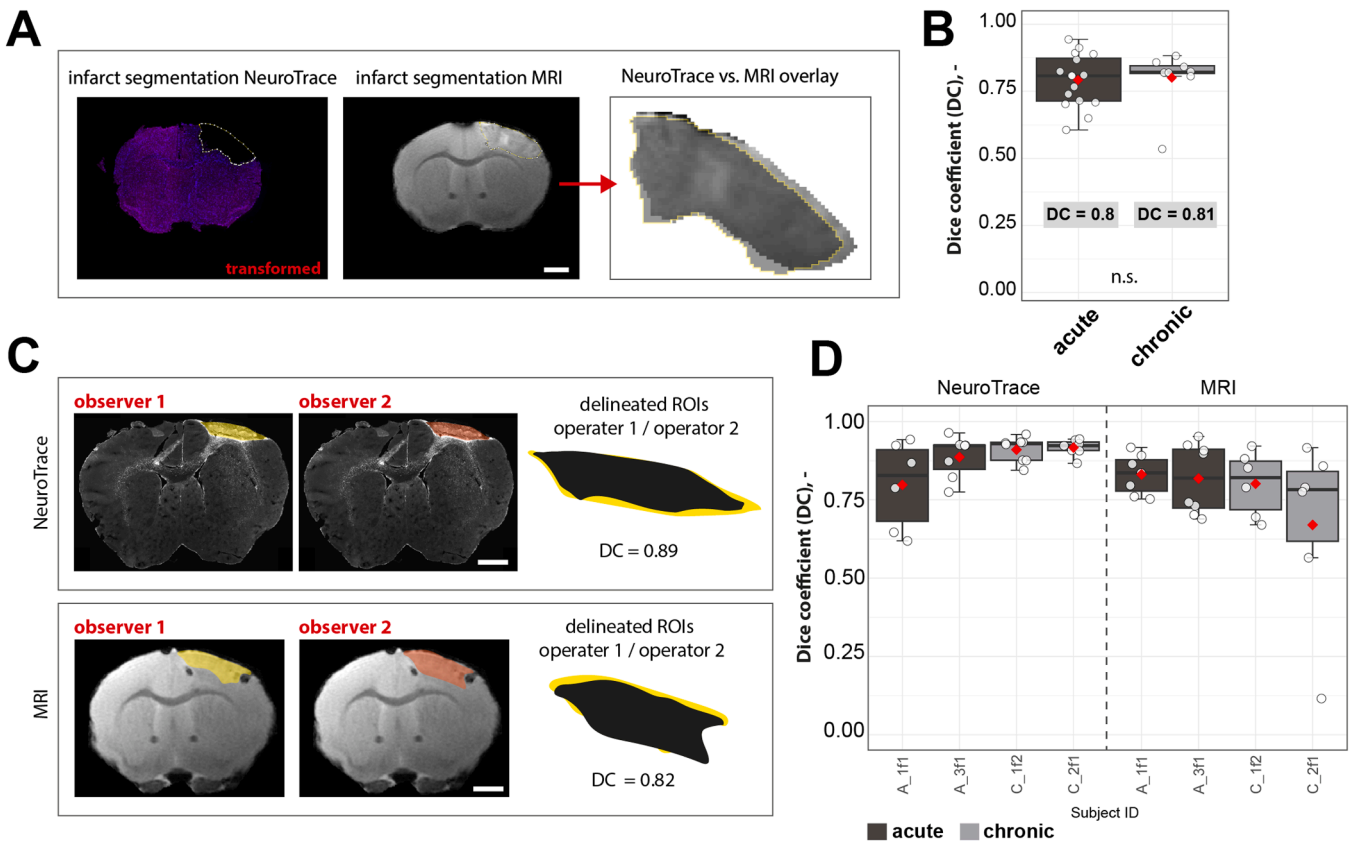

Fig. 5. Correspondence between NeuroTrace- and MRI-delineated ROIs (A-B) and between two operators (C-D) (A) Example of MRI- and NeuroTrace-delineated ROIs (B) DC of lesion ROI delineation in NeuroTrace and MR images; each dot in the plot represents one brain section (C) Examples of MR and NeuroTrace images with manual delineation of lesion ROIs by two observers (D) DC of manual delineation of lesion ROI by two operators; each dot in the plot represents one brain section. Scale bar: 1 mm. Data are shown as mean distributions where the red dot represents the mean. Boxplots indicate the 25 % to 75 % quartiles of the data. Significance of mean differences between the groups (acute vs. chronic) was assessed using unpaired two-sample *t*-test, mean difference between the observer DCs was assessed using a paired two-sample *t*-test. MRI, magnetic resonance imaging; DC, Dice coefficient; ROI, region of interest. .

compared to NeuroTrace-stained sections (DI = 0.89).

MRI provides a three-dimensional and high-resolution view of the brain, which is essential for accurate assessment of stroke size. Even though the use of MRI to image small animals is getting more popular, it is still restricted to well-funded research centers.,(Johnson et al., 2011) A few studies have been conducted to contrast the effectiveness of MRI and histology in experimental stroke models. In a study analyzing multiparametric MRI data after ischemia in rats, a tissue signature analysis demonstrated a high degree of correlation with the histological score at different timepoints (Jacobs et al., 2001) In contrast, others reported that negative MRI (DWI and T2WI) findings 72 h after ischemia may not indicate normal tissue status as seen in the histological outcome (Li et al., 2000) It is possible that the detection of tissue damage by MRI depends on the extent of tissue injury. Partial damage to neurons and glial cells with preservation of tissue structure (known as incomplete infarction) can go unnoticed amidst the seemingly normal cells; and may therefore not be detectable by MRI (Li et al., 2000; Garcia et al., 1997) The ischemic region exhibits distinctive molecular and anatomical features (Rust, 2023), including glial infiltration and the gradual formation of an astrocyte scar, both of which were confirmed in our study. The observed proliferation of astrocytes has been described to reduce T2-weighted signal intensity (Ishii et al., 1998) It is essential to recognize that such alterations in signal characteristics can lead to an underestimation of infarct volume when utilizing MRI for quantifying ischemic damage. Besides increased gliosis, a decrease in water content in the ischemic lesion core and/or resolution of vasogenic edema have been shown to transiently normalize T2 relaxation and thus underestimate stroke-induced damage (Wegener et al., 2006; Lin et al., 2002) It also seems reasonable to assume that the significant variability in MRI protocols, handling and positioning of the animals and postprocessing methods might affect lesion size measurements and therefore complicate the comparison to well-standardized histological measures (Milidonis et al., 2015)

The advantage of *ex-vivo* imaging is that it allows for high-throughput acquisition of multiple sections, providing morphologically detailed data of an entire target organ, while avoiding contamination from physiological sources such as pulse, respiration, swallowing and other movements. The use of *ex vivo* brains can notably increase image resolution and even facilitate additional morphological analysis. Furthermore, the specimen stays intact for follow-up histology. For instance, sliced brain sections can be stained to analyze histological changes associated with regeneration including inflammation, scarring, neurogenesis and vascular repair (Rust et al., 2019; Rust et al., 2020). It has been discussed previously that artefacts due to formalin fixation may have effects on *ex vivo* MRI measurements, such as fractional anisotropy (FA), myelin water fraction (MWF) or on T1- and T2-relaxation times. Formalin fixation of *ex vivo* brain specimens has been shown to cause dehydration and subsequent reduction in the signal-to-noise ratio (SNR) (Shepherd et al., 2009) However, this can be adjusted through increased signal averaging, or normalizing the water diffusion coefficient to the healthy, contralateral hemisphere to standardize lesion-associated changes (Liu et al., 2013; Shereen et al., 2011) Earlier studies reported a reduction in T2-relaxation times during progressive formalin fixation in human brain samples (Shatil et al., 2018) However, it is crucial to acknowledge that this observed effect is intrinsically confounded by extended echo times (>70 ms). In our current study, we employed

shorter echo times (10 ms) as a measure to mitigate the influence of these confounding factors. Future *ex vivo* T2-weighted imaging studies may benefit from further optimizing image SNR by incorporating even shorter echo times (TEs), higher field strengths, or by extending overall scan times (Shatil et al., 2018) SNR efficiency can further be optimized by decreasing fixative concentrations from 4 % to 2 % or, if feasible, by scanning *in situ* (immediately following death), thereby avoiding formalin fixation (Barrett et al., 2023) With these modifications in mind, we believe that *ex vivo* brain imaging can provide quantitative lesion estimates, comparable to *in vivo* MRI data.

Histological methods for lesion evaluation usually include the slicing of brain sections followed by either 2,3,5-triphenyltetrazolium chloride (TTC) staining, haematoxylin and eosin (H&E) staining, or cresyl violet staining. However, many studies demonstrate that TTC staining can be accurately performed as late as seven days after stroke, making it unusable for long-term studies. Another possibility is to immunolabel for specific cellular markers using fixed tissue. Immunolabeling might give rise to images with greater resolution, even down to cellular and subcellular levels. We used NeuroTrace, a fluorescent Nissl stain, to histologically identify the lesioned area. However, there are several other cell markers that can be applied to locate ischemic regions. Neuronal markers such as NeuN (Neuronal Nuclei), MAP2 (Microtubule-Associated Protein 2) or βIII-Tubulin help to distinguish between healthy and damaged neurons. Reactive astrocytes and activated microglia can be identified using GFAP (Glial Fibrillary Acidic Protein) or Iba1 (Ionized calcium-binding adapter molecule 1). These markers are used to locate the glial scar and the ischemic core, respectively (Buscemi et al., 2019) CD31 is a vascular marker that reflects ischemia-induce changes in vasculature, such as endothelial cell swelling or blood brain barrier (BBB) leakage (Weber et al., 2022; Rust et al., 2019) Summing up, the selection of specific markers depends on the research question and the nature of the stroke model being studied.

Preclinical studies emphasize the validity of lesion volume quantification to evaluate the effectiveness of potential treatments for stroke. E.g., cell-based therapy has been demonstrated to reduce infarct volume while improving neurological function deficits in different experimental stroke models. The systemic application of mesenchymal stem cells (MSCs) significantly decreases lesion volumes in different experimental stroke models and the intravenous transplantation of neural progenitor cells (NPCs) leads to a reduction of infarct size along with long-term functional amelioration after ischemia (Bacigaluppi et al., 2016; Bonsack et al., 2020; Chung et al., 2021) Antibody-based treatment strategies have also been proven to effectively reduce infarct volumes and improve neuronal performance in different experimental stroke models (Woods et al., 2020; Rust et al., 2019) Inhibition of TRL4 using monoclonal antibodies decreased both infarct volume and brain swelling in MCAO mice compared to an untreated group (Andresen et al., 2016) Likewise, approaches to regulate angiogenesis (so called pro- and anti-angiogenic therapies) are increasingly being explored (Rust et al., 2019) Ventricular injections of vascular endothelial growth factor (VEGF) have been shown to stimulate angiogenesis and reduce infarct volume in adult rats and the genetic overexpression of VEGF increased brain microvessel density after MCAO in mice (Sun et al., 2003; Wang et al., 2005)

Infarct size is often used as a surrogate measure for functional outcome and has been shown to correlate with e.g. the Bederson score, the forelimb placing performance, the water maze test or overall sensorimotor asymmetry quantification (Bieber et al., 2019; Turner et al., 2016; Machado et al., 2009) However, other attempts to correlate behavior outcomes with infarct volumes have met mixed results, questioning the validity of the assumption that a larger stroke corresponds to more severe neurological deficits (Wakayama et al., 2007; Encarnacion et al., 2011) Consistency in lesion measurement techniques and protocols would allow for more reliable conclusions. Standardization could enable the pooling of data from multiple studies and shed light on the likelihood of volume-function correlations in preclinical research.

Stroke severity extends beyond the mere measurement of infarct volume and long-term outcome is determined by several factors, such as edema formation, postischemic angiogenesis and/or reactive astrogliosis. Postischemic edema formation is a common consequence of stroke and can exacerbate the damage caused by the initial ischemic or hemorrhagic event by increasing intracranial pressure, compromising blood flow, and triggering secondary injury mechanisms (Chen et al., 2021) Edema may increase the brain volume in the infarcted region and thus artificially inflate the apparent size of the lesion volume. Hence, various correction schemes have been developed to correct for the space-occupying effect of brain edema and allow for a more accurate assessment of tissue damage (Lin et al., 1993; McBride et al., 2015; McBride et al., 2016) These schemes are widely accepted for volume measurements on histologically processed images, however, they are generally not applicable to *ex vivo* MRI images. Here, the intact skull acts as an external barrier hindering the intracranial pressure from being released whereas histological examination requires the opening of the skull (Koch et al., 2019) The comparison of edema-correction schemes for both histologically processed and MR images should be considered in future studies.

Post-stroke angiogenesis is thought to play a key role during restorative processes after an ischemic insult and leads to improved functional and neurological outcomes. However, only few studies assessed if increased cerebral blood flow in tissue surrounding the infarcted area also directly coincides with a decrease in lesion volume. VEGF, a pro-angiogenic molecule, shows high upregulation as early as 3 h after an ischemic insult and has been shown to alleviate neurological deficits and infarct volume (Wang et al., 2005; Reitmeir et al., 2012) However, it has also been asserted that VEGF triggers vascular permeability and administration of exogenous VEGF may even lead to increased infarct volume, further questioning the impact of postischemic angiogenesis on lesion volume development.

In our study, no vascular differences were observed between the acute and the chronic phase, even though infarct volume significantly decreased over this time course. Hence, we could also not confirm a positive association between postischemic angiogenesis and reduced infarct volume. Angiogenesis typically starts 3 – 4 days after ischemia but may occur transiently. Recent evidence suggests that the post-ischemic angiogenic-signaling cascade is rather used to synthesize microvessels needed for macrophage infiltration that contribute to the clearing up of cellular debris (Manoonkitiwongsa et al., 2001; Yu et al., 2007) Once these newly formed vessels have fulfilled their purpose, they undergo degradation and might not be detectable anymore as late as 28 days after injury onset.

Alterations in astrocytes following stroke are widely recognized. However, it remains debated whether GFAP-positive astrocytes act as promotors of regeneration or contribute as detrimental factors in the aftermath of a stroke (Akhoundzadeh and Shafia, 2021) In line with previous research, we have shown a significant increase in GFAP-positive astrocytes over a time course of 3 weeks after ischemia induction (Buscemi et al., 2019; Parker et al., 2017; Hao et al., 2016) There is a vast number of studies that show a clear association between the postischemic increase in GFAP-positive astrocytes and a decline in lesion size, along with improved functional recovery; however, we could not confirm a positive nor a negative relationship between GFAP-levels and MRI-obtained infarct volumes (Parker et al., 2017; Liebigt et al., 2012; Borlongan et al., 2000) Elevated levels of GFAP expression appear to be a potential neurobiological mechanism that contributes to the amelioration of functional deficits caused by an ischemic infarct. Thus, therapeutic interventions aiming at modulating reactive astrocytes could prove beneficial (Akhoundzadeh and Shafia, 2021) Along with other positive effects, astrocytes contribute to glutamate homeostasis in the CNS, restore BBB integrity, serve as anti-inflammatory barrier, and shield the healthy tissue from further harm (Pekny and Pekna, 2016) However, the results about the relationship between GFAP expression and lesion volume decrease are inconclusive as other studies strongly

suggest that astrogliosis is a malevolent factor in stroke complications (Badan et al., 2003; Popa-Wagner et al., 2006; Liu and Geng, 2018) The formation of a glial scar can have a detrimental impact on long-term outcomes due to its inhibitory properties (Barreto et al., 2011) Therapeutic interventions to reduce glial scar thickness have proven beneficial and resulted in significant improvement in neurological outcome along with reduced lesion volume (Li et al., 2005) Taken together, GFAP positive cells may exert both, harmful and helpful effects on stroke outcomes. Some studies expressed that the mode of action of reactive astrocytes depends on time point of stroke, extend of damage and the severity of inflammation (Pekny and Pekna, 2016; Barreto et al., 2011) In addition, the observed variability in astrocytic response to brain injury is likely influenced by variations in stroke induction models and/or the duration of ischemia. To elucidate the exact role of reactive astrocytes in stroke outcome and their impact on lesion volume development, more studies are needed.

The combination of *ex vivo* MRI and histopathology should be considered, not only for analyzing lesion dimensions but also for other neurological research questions. Due to the brain's heterogeneity, histological sectioning often fails to provide a complete view of every region. MRI on a fixed brain could guide pathologists to sample specific areas for subsequent work-up (Hanig et al., 2014) For stem cell applications, preclinical assessments are required to test for potential tumor induction. *Ex vivo* MRI can be used to scan the brain and the spinal cord following cell injection to identify specific (abnormal pale) areas, which potentially correlate histopathologically to teratomas (Ramot et al., 2017) Using both MRI paired with gross histological will optimize time of sacrifice and selection of an appropriate stain and improve the scientific significance of the experimental data.

The photothrombotic model of stroke is a well-standardized model that has many strengths, including consistent location and size of infarct, relatively simple surgical procedures, and a low mortality rate (Labat-gest and Tomasi, 2013; Sun et al., 2020) Despite being a rather mild model compared to other experimental stroke models such as MCAO, we found a robust loss of neurons in the infarcted regions and well-defined ischemic border zones. This is consistent with own findings from previous studies, where we additionally showed that neuronal loss is usually accompanied by fewer astrocytes and decreased microglia activation in the stroke core zone (Weber et al., 2020; Weber et al., 2022) The infarct volumes and cortical depths observed in this study are comparable to previous studies that have used the photothrombotic stroke model (Porritt et al., 2012; Kaiser et al., 2019; Aswendt et al., 2021) The lesion developed into deep cortical layers (from layer IV to layer VI) across all animals, but no subcortical areas were affected. These morphological cortical tissue changes are not confined solely to the photothrombotic stroke model but have also been described after distal MCA occlusion (Minassian et al., 2019)However, experimental methods such as occlusion models or procedures using vasoconstrictive agents (e.g., ET-1) typically affect larger portions of the brain including subcortical areas and can cause severe neurological deficits. Especially the latter one induces infarcts of variable sizes in nearly any brain, making it more difficult to standardize compared to the photothrombotic model (Sommer, 2017)

In conclusion, we describe a toolkit that allows straightforward lesion volume estimation of ischemic mouse brains. This toolkit generates results that are highly correlated when assessing stroke volumes, whether using full brain MRI images or sliced NeuroTrace-stained brain sections at acute and chronic time points after stroke.

CRediT authorship contribution statement

Rebecca Z. Weber: Writing – review & editing, Writing – original draft, Formal analysis, Data curation, Conceptualization. **Davide Bernardoni:** Software, Resources, Methodology, Formal analysis, Data curation. **Nora H. Rentsch:** Formal analysis, Data curation. **Beatriz Achón Buil:** Formal analysis, Data curation. **Stefanie Halliday:** Formal analysis, Data curation. **Mark-Aurel Augath:** Formal analysis, Data curation. **Daniel Razansky:** Writing – review & editing, Writing – original draft, Validation, Supervision, Resources, Formal analysis, Conceptualization. **Christian Tackenberg:** Writing – review & editing, Writing – original draft, Visualization, Validation, Supervision, Resources, Methodology, Investigation, Funding acquisition, Formal analysis, Data curation, Conceptualization. **Ruslan Rust:** Writing – review & editing, Writing – original draft, Visualization, Validation, Supervision, Software, Resources, Project administration, Methodology, Investigation, Funding acquisition, Formal analysis, Data curation, Conceptualization.

Declaration of competing interest

The authors declare that the research was conducted in the absence of any commercial or financial relationships that could be construed as a potential conflict of interest.

Data availability

Data will be made available on request.

Acknowledgment

None.

Supplementary materials

Supplementary material associated with this article can be found, in the online version, at doi:10.1016/j.neuroimage.2024.120518.

References

Heart Disease and Stroke Statistics—2016 Update | Circulation. Accessed April 18, 2023. https://www.ahajournals.org/doi/10.1161/CIR.0000000000000350?url_ver=Z39.88-2003&rfr_id=ori:rid:crossref.org&rfr_dat=cr_pub%20%200pubmed.

McDermott, M., Skolarus, L.E., Burke, J.F., 2019. A systematic review and meta-analysis of interventions to increase stroke thrombolysis. BMC Neurol. 19 (1), 86. https://doi.org/10.1186/s12883-019-1298-2.

Lourbopoulos, A., Mourouzis, I., Xinaris, C., et al., 2021. Translational block in stroke: a constructive and "out-of-the-box" reappraisal. Front. Neurosci. 15, 652403 https://doi.org/10.3389/fnins.2021.652403.

Ludewig, P., Gdaniec, N., Sedlacik, J., et al., 2017. Magnetic particle imaging for real-time perfusion imaging in acute stroke. ACS Nano 11 (10), 10480–10488. https://doi.org/10.1021/acsnano.7b05784.

Mulder, I.A., Khmelinskii, A., Dzyubachyk, O., et al., 2017. Automated ischemic lesion segmentation in MRI mouse brain data after transient middle cerebral artery occlusion. Front. Neuroinform. 11. Accessed April 18, 2023. https://www.frontiersin.org/articles/10.3389/fninf.2017.00003.

García-Cabezas, M.Á., John, Y.J., Barbas, H., Zikopoulos, B., 2016. Distinction of neurons, glia and endothelial cells in the cerebral cortex: an algorithm based on cytological features. Front. Neuroanat. 10. Accessed April 18, 2023. https://www.frontiersin.org/articles/10.3389/fnana.2016.00107.

Atochin, D.N., Chernysheva, G.A., Aliev, O.I., et al., 2017. An improved three-vessel occlusion model of global cerebral ischemia in rats. Brain Res. Bull. 132, 213–221. https://doi.org/10.1016/j.brainresbull.2017.06.005.

Choi, C.H., Yi, K.S., Lee, S.R., et al., 2018. A novel voxel-wise lesion segmentation technique on 3.0-T diffusion MRI of hyperacute focal cerebral ischemia at 1 h after permanent MCAO in rats. J. Cereb. Blood Flow Metab. 38 (8), 1371–1383. https://doi.org/10.1177/0271678x17714179.

Bay, V., Iversen, N.K., Shiadeh, S.M.J., Tasker, R.A., Wegener, G., Ardalan, M., 2021. Tissue processing and optimal visualization of cerebral infarcts following sub-acute focal ischemia in rats. J. Chem. Neuroanat. 118, 102034 https://doi.org/10.1016/j.jchemneu.2021.102034.

Schindelin, J., Arganda-Carreras, I., Frise, E., et al., 2012. Fiji: an open-source platform for biological-image analysis. Nat. Methods 9 (7), 676–682. https://doi.org/10.1038/nmeth.2019.

Sommer, C., 2010. Histology and infarct volume determination. Dirnagl U, ed Rodent Models of Stroke 213–226. https://doi.org/10.1007/978-1-60761-750-1_15.

Raylman, R.R., Ledden, P., Stolin, A.V., Hou, B., Jaliparthi, G., Martone, P.F., 2018. Small animal, positron emission tomography-magnetic resonance imaging system based on a clinical magnetic resonance imaging scanner: evaluation of basic imaging performance. J. Med. Imaging 5 (3), 033504. https://doi.org/10.1117/1.JMI.5.3.033504.

Gabrielson, K., Maronpot, R., Monette, S., et al., 2018. *In vivo* imaging with confirmation by histopathology for increased rigor and reproducibility in translational research: a review of examples, options, and resources. ILAR J. 59 (1), 80–98. https://doi.org/10.1093/ilar/ily010.

Bogaert-Buchmann, A., Poittevin, M., Po, C., et al., 2013. Spatial and temporal MRI profile of ischemic tissue after the acute stages of a permanent mouse model of stroke. Open Neuroimaging J. 7, 4–14. https://doi.org/10.2174/1874440001307010004.

Weber, R.Z., Grönnert, L., Mulders, G., et al., 2020. Characterization of the blood brain barrier disruption in the photothrombotic stroke model. Front. Physiol. 11. Accessed April 18, 2023. https://www.frontiersin.org/articles/10.3389/fphys.2020.586226.

Rust, R., Grönnert, L., Gantner, C., et al., 2019a. Nogo-A targeted therapy promotes vascular repair and functional recovery following stroke. Proc. Natl. Acad. Sci. 116 (28), 14270–14279. https://doi.org/10.1073/pnas.1905309116.

Rust, R., Weber, R.Z., Grönnert, L., et al., 2019b. Anti-Nogo-A antibodies prevent vascular leakage and act as pro-angiogenic factors following stroke. Sci. Rep. 9 (1), 1–10. https://doi.org/10.1038/s41598-019-56634-1.

Fan, Z., Ardicoglu, R., Batavia, A.A., et al., 2023. The vascular gene Apold1 is dispensable for normal development but controls angiogenesis under pathological conditions. Angiogenesis 18. https://doi.org/10.1007/s10456-023-09870-z. Published online March.

Weber, R.Z., Mulders, G., Kaiser, J., Tackenberg, C., Rust, R., 2022a. Deep learning-based behavioral profiling of rodent stroke recovery. BMC Biol. 20 (1), 232. https://doi.org/10.1186/s12915-022-01434-9.

Rust, R., Weber, R.Z., Generali, M., et al., 2022. Xeno-free induced pluripotent stem cell-derived neural progenitor cells for *in vivo* applications. J. Transl. Med. 20 (1), 421. https://doi.org/10.1186/s12967-022-03610-5.

Sergejeva, M., Papp, E.A., Bakker, R., et al., 2015. Anatomical landmarks for registration of experimental image data to volumetric rodent brain atlasing templates. J. Neurosci. Methods 240, 161–169. https://doi.org/10.1016/j.jneumeth.2014.11.005.

Saalfeld S., Tomancak P. 2023 Automatic landmark correspondence detection for ImageJ.

Rust, R., Grönnert, L., Dogançay, B., Schwab, M.E., 2019c. A revised view on growth and remodeling in the retinal vasculature. Sci. Rep. 9 (1), 3263. https://doi.org/10.1038/s41598-019-40135-2.

Gouveia, A., Seegobin, M., Kannangara, T.S., et al., 2017. The aPKC-CBP pathway regulates post-stroke neurovascular remodeling and functional recovery. Stem Cell Rep. 9 (6), 1735–1744. https://doi.org/10.1016/j.stemcr.2017.10.021.

Wahl, A.S., Büchler, U., Brändli, A., et al., 2017. Optogenetically stimulating intact rat corticospinal tract post-stroke restores motor control through regionalized functional circuit formation. Nat. Commun. 8 (1), 1187. https://doi.org/10.1038/s41467-017-01090-6.

Reference Atlas: Allen Brain Atlas: mouse Brain. Accessed April 18, 2023. https://mouse.brain-map.org/static/atlas.

Koch, S., Mueller, S., Foddis, M., et al., 2019. Atlas registration for edema-corrected MRI lesion volume in mouse stroke models. J. Cereb. Blood Flow Metab. 39 (2), 313–323. https://doi.org/10.1177/0271678x17726635.

Modified Akima piecewise cubic Hermite interpolation - MATLAB makima. Accessed April 18, 2023. https://www.mathworks.com/help/matlab/ref/makima.html.

Gaudinski, M.R., Henning, E.C., Miracle, A., Luby, M., Warach, S., Latour, L.L., 2008. Establishing final infarct volume. Stroke 39 (10), 2765–2768. https://doi.org/10.1161/STROKEAHA.107.512269.

Li, H., Zhang, N., Lin, H.Y., et al., 2014. Histological, cellular and behavioral assessments of stroke outcomes after photothrombosis-induced ischemia in adult mice. BMC Neurosci. 15 (1), 58. https://doi.org/10.1186/1471-2202-15-58.

Shen, F., Jiang, L., Han, F., Degos, V., Chen, S., Su, H., 2019. Increased inflammatory response in old mice is associated with more severe neuronal injury at the acute stage of ischemic stroke. Aging Dis. 10 (1), 12–22. https://doi.org/10.14336/AD.2018.0205.

Pianta, S., Lee, J.Y., Tuazon, J.P., et al., 2019. A short bout of exercise prior to stroke improves functional outcomes by enhancing angiogenesis. Neuromol. Med. 21 (4), 517–528. https://doi.org/10.1007/s12017-019-08533-x.

Vahid-Ansari, F., Lagace, D.C., Albert, P.R., 2016. Persistent post-stroke depression in mice following unilateral medial prefrontal cortical stroke. Transl. Psychiatry 6 (8), e863. https://doi.org/10.1038/tp.2016.124.

McBride, D.W., Tang, J., Zhang, J.H., 2016. Development of an infarct volume algorithm to correct for brain swelling after ischemic stroke in rats. Acta Neurochir. Suppl. 121, 103–109. https://doi.org/10.1007/978-3-319-18497-5_18.

An, J., Wendt, L., Wiese, G., et al., 2023. Deep learning-based automated lesion segmentation on mouse stroke magnetic resonance images. Sci. Rep. 13 (1), 13341. https://doi.org/10.1038/s41598-023-39826-8.

Sørensen T., Sørensen T., Biering-Sørensen T., Sørensen T., Sorensen J.T. A method of establishing group of equal amplitude in plant sociobiology based on similarity of species content and its application to analyses of the vegetation on Danish commons. In:; 1948. Accessed October 3, 2023. https://www.semanticscholar.org/paper/A-method-of-establishing-group-of-equal-amplitude-S%C3%B8rensen-S%C3%B8rensen/d8d3e6d95b60ec6ac8f91f42a6914a87b13a6bc1.

Zou, K.H., Wells, W.M., Kikinis, R., Warfield, S.K., 2004. Three validation metrics for automated probabilistic image segmentation of brain tumours. Stat. Med. 23 (8), 1259–1282. https://doi.org/10.1002/sim.1723.

Johnson, G.A., Badea, A., Jiang, Y., 2011. Quantitative neuromorphometry using magnetic resonance histology. Toxicol. Pathol. 39 (1), 85–91. https://doi.org/10.1177/0192623310389622.

Jacobs, M.A., Zhang, Z.G., Knight, R.A., et al., 2001. A model for multiparametric mri tissue characterization in experimental cerebral ischemia with histological validation in rat: part 1. Stroke 32 (4), 943–949. https://doi.org/10.1161/01.str.32.4.943.

Li, F., Liu, K.F., Silva, M.D., et al., 2000. Transient and permanent resolution of ischemic lesions on diffusion-weighted imaging after brief periods of focal ischemia in rats : correlation with histopathology. Stroke 31 (4), 946–954. https://doi.org/10.1161/01.str.31.4.946.

Garcia, J.H., Liu, K.F., Ye, Z.R., Gutierrez, J.A., 1997. Incomplete infarct and delayed neuronal death after transient middle cerebral artery occlusion in rats. Stroke 28 (11), 2303–2309. https://doi.org/10.1161/01.str.28.11.2303 discussion 2310.

Rust, R., 2023. Ischemic stroke-related gene expression profiles across species: a meta-analysis. J. Inflamm. 20 (1), 21. https://doi.org/10.1186/s12950-023-00346-x.

Ishii, H., Arai, T., Morikawa, S., et al., 1998. Evaluation of focal cerebral ischemia in rats by magnetic resonance imaging and immunohistochemical analyses. J. Cereb. Blood Flow Metab. 18 (9), 931–934. https://doi.org/10.1097/00004647-199809000-00001.

Wegener, S., Hoehn, M., Back, T., 2006. Ischemic edema and necrosis. Von Kummer Rü, B T Magnetic Resonance Imaging in Ischemic Stroke. Medical Radiology. Springer, Berlin Heidelberg, pp. 133–148. https://doi.org/10.1007/3-540-27738-2_8.

Lin, S.P., Schmidt, R.E., McKinstry, R.C., Ackerman, J.J.H., Neil, J.J., 2002. Investigation of mechanisms underlying transient T2 normalization in longitudinal studies of ischemic stroke. J. Magn. Reson. Imaging JMRI 15 (2), 130–136. https://doi.org/10.1002/jmri.10052.

Milidonis, X., Marshall, I., Macleod, M.R., Sena, E.S., 2015. Magnetic resonance imaging in experimental stroke and comparison with histology. Stroke 46 (3), 843–851. https://doi.org/10.1161/STROKEAHA.114.007560.

Rust, R., Kirabali, T., Grönnert, L., et al., 2020. A practical guide to the automated analysis of vascular growth, maturation and injury in the brain. Front. Neurosci. 14 https://doi.org/10.3389/fnins.2020.00244.

Shepherd, T.M., Thelwall, P.E., Stanisz, G.J., Blackband, S.J., 2009. Aldehyde fixative solutions alter the water relaxation and diffusion properties of nervous tissue. Magn. Reson. Med. 62 (1), 26–34. https://doi.org/10.1002/mrm.21977.

Liu, Y., Sajja, B.R., Gendelman, H.E., Boska, M.D., 2013. Mouse brain fixation to preserve *in vivo* manganese enhancement for *ex vivo* manganese-enhanced MRI. J. Magn. Reson. Imaging JMRI 38 (2), 482–487. https://doi.org/10.1002/jmri.24005.

Shereen, A., Nemkul, N., Yang, D., et al., 2011. *Ex vivo* diffusion tensor imaging and neuropathological correlation in a murine model of hypoxia–ischemia-induced thrombotic stroke. J. Cereb Blood Flow Metab. 31 (4), 1155–1169. https://doi.org/10.1038/jcbfm.2010.212.

Shatil, A.S., Uddin, M.N., Matsuda, K.M., Figley, C.R., 2018. Quantitative *ex vivo* MRI changes due to progressive formalin fixation in whole human brain specimens: longitudinal characterization of diffusion, relaxometry, and myelin water fraction measurements at 3T. Front. Med. 5. Accessed December 5, 2023. https://www.frontiersin.org/articles/10.3389/fmed.2018.00031.

Barrett, R.L.C., Cash, D., Simmons, C., et al., 2023. Tissue optimization strategies for high-quality *ex vivo* diffusion imaging. Nmr Biomed. 36 (3), e4866. https://doi.org/10.1002/nbm.4866.

Buscemi, L., Price, M., Bezzi, P., Hirt, L., 2019. Spatio-temporal overview of neuroinflammation in an experimental mouse stroke model. Sci. Rep. 9 (1), 507. https://doi.org/10.1038/s41598-018-36598-4.

Weber, R.Z., Mulders, G., Perron, P., Tackenberg, C., Rust, R., 2022b. Molecular and anatomical roadmap of stroke pathology in immunodeficient mice. Front. Immunol. 13. Accessed April 19, 2023. https://www.frontiersin.org/articles/10.3389/fimmu.2022.1080482.

Bacigaluppi, M., Russo, G.L., Peruzzotti-Jametti, L., et al., 2016. Neural stem cell transplantation induces stroke recovery by upregulating glutamate transporter GLT-1 in astrocytes. J. Neurosci. 36 (41), 10529–10544. https://doi.org/10.1523/JNEUROSCI.1643-16.2016.

Bonsack, B., Corey, S., Shear, A., et al., 2020. Mesenchymal stem cell therapy alleviates the neuroinflammation associated with acquired brain injury. CNS Neurosci. Ther. 26 (6), 603–615. https://doi.org/10.1111/cns.13378.

Chung, J.W., Chang, W.H., Bang, O.Y., et al., 2021. Efficacy and safety of intravenous mesenchymal stem cells for ischemic stroke. Neurology 96 (7), e1012–e1023. https://doi.org/10.1212/WNL.0000000000011440.

Woods, D., Jiang, Q., Chu, X.P., 2020. Monoclonal antibody as an emerging therapy for acute ischemic stroke. Int. J. Physiol. Pathophysiol. Pharmacol. 12 (4), 95–106.

Andresen, L., Theodorou, K., Grünewald, S., et al., 2016. Evaluation of the therapeutic potential of anti-TLR4-antibody MTS510 in experimental stroke and significance of different routes of application. PLoS ONE 11 (2), e0148428. https://doi.org/10.1371/journal.pone.0148428.

Rust, R., Gantner, C., Schwab, M.E., 2019d. Pro- and antiangiogenic therapies: current status and clinical implications. FASEB J. 33 (1), 34–48. https://doi.org/10.1096/fj.201800640RR.

Sun, Y., Jin, K., Xie, L., et al., 2003. VEGF-induced neuroprotection, neurogenesis, and angiogenesis after focal cerebral ischemia. J. Clin. Invest. 111 (12), 1843–1851. https://doi.org/10.1172/JCI17977.

Wang, Y., Kilic, E., Kilic, U., et al., 2005. VEGF overexpression induces post-ischaemic neuroprotection, but facilitates haemodynamic steal phenomena. Brain J. Neurol. 128 (Pt 1), 52–63. https://doi.org/10.1093/brain/awh325.

Bieber, M., Gronewold, J., Scharf, A.C., et al., 2019. Validity and reliability of neurological scores in mice exposed to middle cerebral artery occlusion. Stroke 50 (10), 2875–2882. https://doi.org/10.1161/STROKEAHA.119.026652.

C Turner, R., DiPasquale, K., F Logsdon, A., et al., 2016. The role for infarct volume as a surrogate measure of functional outcome following ischemic stroke. J. Syst. Integr. Neurosci. 2 (4) https://doi.org/10.15761/JSIN.1000136.

Machado, A.G., Baker, K.B., Schuster, D., Butler, R.S., Rezai, A., 2009. Chronic electrical stimulation of the contralesional lateral cerebellar nucleus enhances recovery of

motor function after cerebral ischemia in rats. Brain Res. 1280, 107–116. https://doi.org/10.1016/j.brainres.2009.05.007.
Wakayama, K., Shimamura, M., Sata, M., et al., 2007. Quantitative measurement of neurological deficit after mild (30min) transient middle cerebral artery occlusion in rats. Brain Res. 1130 (1), 181–187. https://doi.org/10.1016/j.brainres.2006.10.088.
Encarnacion, A., Horie, N., Keren-Gill, H., Bliss, T.M., Steinberg, G.K., Shamloo, M., 2011. Long-term behavioral assessment of function in an experimental model for ischemic stroke. J. Neurosci. Methods 196 (2), 247–257. https://doi.org/10.1016/j.jneumeth.2011.01.010.
Chen, S., Shao, L., Ma, L., 2021. Cerebral edema formation after stroke: emphasis on blood–brain barrier and the lymphatic drainage system of the brain. Front. Cell Neurosci. 15, 716825 https://doi.org/10.3389/fncel.2021.716825.
Lin, T.N., He, Y.Y., Wu, G., Khan, M., Hsu, C.Y., 1993. Effect of brain edema on infarct volume in a focal cerebral ischemia model in rats. Stroke 24 (1), 117–121. https://doi.org/10.1161/01.str.24.1.117.
McBride, D.W., Klebe, D., Tang, J., Zhang, J.H., 2015. Correcting for brain swelling's effects on infarct volume calculation after middle cerebral artery occlusion in rats. Transl. Stroke Res. 6 (4), 323–338. https://doi.org/10.1007/s12975-015-0400-3.
Reitmeir, R., Kilic, E., Reinboth, B.S., et al., 2012. Vascular endothelial growth factor induces contralesional corticobulbar plasticity and functional neurological recovery in the ischemic brain. Acta Neuropathol. 123 (2), 273–284. https://doi.org/10.1007/s00401-011-0914-z (Berl).
Manoonkitiwongsa, P.S., Jackson-Friedman, C., McMillan, P.J., Schultz, R.L., Lyden, P.D., 2001. Angiogenesis after stroke is correlated with increased numbers of macrophages: the clean-up hypothesis. J. Cereb. Blood Flow Metab. 21 (10), 1223–1231. https://doi.org/10.1097/00004647-200110000-00011.
Yu, S.W., Friedman, B., Cheng, Q., Lyden, P.D., 2007. Stroke-evoked angiogenesis results in a transient population of microvessels. J. Cereb. Blood Flow Metab. Off. J. Int. Soc. Cereb. Blood Flow Metab. 27 (4), 755–763. https://doi.org/10.1038/sj.jcbfm.9600378.
Akhoundzadeh, K., Shafia, S., 2021. Association between GFAP-positive astrocytes with clinically important parameters including neurological deficits and/or infarct volume in stroke-induced animals. Brain Res. 1769, 147566 https://doi.org/10.1016/j.brainres.2021.147566.
Parker, K., Berretta, A., Saenger, S., et al., 2017. PEGylated insulin-like growth factor-I affords protection and facilitates recovery of lost functions post-focal ischemia. Sci. Rep. 7 (1), 241. https://doi.org/10.1038/s41598-017-00336-z.
Hao, X.Z., Yin, L.K., Zhang, X.X., et al., 2016. Combining systemic and stereotactic MEMRI to detect the correlation between gliosis and neuronal connective pathway at the chronic stage after stroke. J. Neuroinflammation 13 (1), 156. https://doi.org/10.1186/s12974-016-0622-7.
Liebigt, S., Schlegel, N., Oberland, J., Witte, O.W., Redecker, C., Keiner, S., 2012. Effects of rehabilitative training and anti-inflammatory treatment on functional recovery and cellular reorganization following stroke. Exp. Neurol. 233 (2), 776–782. https://doi.org/10.1016/j.expneurol.2011.11.037.
Borlongan, C.V., Yamamoto, M., Takei, N., et al., 2000. Glial cell survival is enhanced during melatonin-induced neuroprotection against cerebral ischemia. FASEB J. Off. Publ. Fed Am. Soc. Exp. Biol. 14 (10), 1307–1317. https://doi.org/10.1096/fj.14.10.1307.
Pekny, M., Pekna, M., 2016. Reactive gliosis in the pathogenesis of CNS diseases. Biochim. Biophys. Acta 1862 (3), 483–491. https://doi.org/10.1016/j.bbadis.2015.11.014.
Badan, I., Buchhold, B., Hamm, A., et al., 2003. Accelerated glial reactivity to stroke in aged rats correlates with reduced functional recovery. J. Cereb. Blood Flow Metab. Off. J. Int. Soc. Cereb. Blood Flow Metab. 23 (7), 845–854. https://doi.org/10.1097/01.WCB.0000071883.63724.A7.
Popa-Wagner, A., Dinca, I., Yalikun, S., Walker, L., Kroemer, H., Kessler, C., 2006. Accelerated delimitation of the infarct zone by capillary-derived nestin-positive cells in aged rats. Curr. Neurovasc. Res. 3 (1), 3–13. https://doi.org/10.2174/156720206775541732.
Liu, G., Geng, J., 2018. Glial fibrillary acidic protein as a prognostic marker of acute ischemic stroke. Hum. Exp. Toxicol. 37 (10), 1048–1053. https://doi.org/10.1177/0960327117751236.
Barreto, G., White, R.E., Ouyang, Y., Xu, L., Giffard, R.G., 2011. Astrocytes: targets for neuroprotection in stroke. Cent. Nerv. Syst. Agents Med. Chem. 11 (2), 164–173.
Li, Y., Chen, J., Zhang, C.L., et al., 2005. Gliosis and brain remodeling after treatment of stroke in rats with marrow stromal cells. Glia 49 (3), 407–417. https://doi.org/10.1002/glia.20126.
Hanig, J., Paule, M.G., Ramu, J., et al., 2014. The use of MRI to assist the section selections for classical pathology assessment of neurotoxicity. Regul. Toxicol. Pharmacol. RTP 70 (3), 641–647. https://doi.org/10.1016/j.yrtph.2014.09.010.
Ramot, Y., Schiffenbauer, Y.S., Amouyal, N., et al., 2017. Compact MRI for the detection of teratoma development following intrathecal human embryonic stem cell injection in NOD-SCID mice. Neurotoxicology 59, 27–32. https://doi.org/10.1016/j.neuro.2017.01.003.
Labat-gest, V., Tomasi, S., 2013. Photothrombotic ischemia: a minimally invasive and reproducible photochemical cortical lesion model for mouse stroke studies. J. Vis. Exp. JoVE (76), 50370. https://doi.org/10.3791/50370.
Sun, Y.Y., Kuo, Y.M., Chen, H.R., Short-Miller, J.C., Smucker, M.R., Kuan, C.Y., 2020. A murine photothrombotic stroke model with an increased fibrin content and improved responses to tPA-lytic treatment. Blood Adv. 4 (7), 1222–1231. https://doi.org/10.1182/bloodadvances.2019000782.
Porritt, M.J., Andersson, H.C., Hou, L., et al., 2012. Photothrombosis-induced infarction of the mouse cerebral cortex is not affected by the Nrf2-activator sulforaphane. PLoS ONE 7 (7), e41090. https://doi.org/10.1371/journal.pone.0041090.
Kaiser, J., Maibach, M., Salpeter, I., et al., 2019. The spinal transcriptome after cortical stroke: in search of molecular factors regulating spontaneous recovery in the spinal cord. J. Neurosci. 39 (24), 4714–4726. https://doi.org/10.1523/JNEUROSCI.2571-18.2019.
Aswendt, M., Pallast, N., Wieters, F., Baues, M., Hoehn, M., Fink, G.R., 2021. Lesion size- and location-dependent recruitment of contralesional thalamus and motor cortex facilitates recovery after stroke in mice. Transl. Stroke Res. 12 (1), 87–97. https://doi.org/10.1007/s12975-020-00802-3.
Minassian, A., Dobrivojevic Radmilovic, M., Vogel, S., et al., 2019. Cortical tissue loss and major structural reorganization as result of distal middle cerebral artery occlusion in the chronic phase of nude mice. Sci. Rep. 9 (1), 6823. https://doi.org/10.1038/s41598-019-43341-0.
Sommer, C.J., 2017. Ischemic stroke: experimental models and reality. Acta Neuropathol. 133 (2), 245–261. https://doi.org/10.1007/s00401-017-1667-0 (Berl).